IEEE Access
Multidisciplinary ⋮ Rapid Review ⋮ Open Access Journal

Received February 1, 2021, accepted February 19, 2021, date of publication February 23, 2021, date of current version March 4, 2021.

Digital Object Identifier 10.1109/ACCESS.2021.3061461

Minimum Power Density Criterion Based Relay Selection and Power Allocation for Wireless Avionics Intra-Communications

YUANJUN ZUO, (Graduate Student Member, IEEE), QIAO LI, (Member, IEEE), GUANGSHAN LU, AND HUAGANG XIONG

School of Electronic and Information Engineering, Beihang University, Beijing 100191, China

Corresponding author: Qiao Li (avionics@buaa.edu.cn)

This work was supported by the National Natural Science Foundation of China under Grant 62071023.

ABSTRACT Wireless relay technology improves information capacity and brings diversity gain for wireless avionics intra-communications (WAIC) which will replace some cabling interconnections in aircraft. An amplify-and-forward(AF) relay selection scheme considering transmitter power level in the cabin has been proposed, with physical layer of multi-band Orthogonal Frequency-Division Multiplexing Ultra-wide band (MB-OFDM-UWB), of which outage probability performance is characterized in terms of the cluster and ray arrival rates. Furthermore, minimum power density principle based relay selection and power allocation scheme (MPRP) has been proposed to mitigate the limitation. In particular, Quasi-Newton method is used to solve nonlinear systems in the calculation of power distribution factor. Simulation results demonstrate that the proposed MPRP scheme achieves the optimized system energy efficiency.

INDEX TERMS Outage probability, relay selection, UWB, WAIC, wireless communication.

I. INTRODUCTION

A. WIRELESS AVIONICS INTRA-COMMUNICATION

The existing avionics systems such as 1553B bus and AFDX (Avionics Full Duplex Switched Ethernet) network are interconnected by a large number of cables. Cabling avionics system cost significantly to the aircraft manufacturer, operator, and other flying publics. The production cost consists of the wiring design, installation, and maintenance. The wiring system gives 2-5% weight of aircraft. The routing plan in the cable design on the aircraft could reach approximately 280 miles or 450.62 kilometers long [1]. Therefore, the aviation industry and the aerospace community are studying in the scope of varied projects on wireless systems [2]–[4]. These projects will be helpful in the next generation of aircraft and contribute to reduce the number of interconnecting wires on board. Wireless technology can not only reduce the weight of cables and thus reduce the fuel consumption [5], but also save the time and cost related to cabling design and installation [6]. In addition, wireless technology can also improve the communication redundancy, so as to improve the reliability and scalability of the system [7].

The associate editor coordinating the review of this manuscript and approving it for publication was Wenchi Cheng.

In order to meet these application requirements, a lot of research has been carried out. The aviation industry and the International Telecommunication Union (ITU) are actually developing a new wireless system called WAIC (Wireless Avionics Intra-Communication) [8]. WAIC is restricted to applications related to secure, reliable, and effective aircraft operations such as structural health monitoring, sensing [9], and fieldbus communications [10], as defined by the International Civil Aviation Organization (ICAO). And AVSI (Aerospace Vehicle Systems Institute) divided WAIC systems into 4 categories based on data rate requirement and transceiver location. The 4 categories are HI (high data rate inside), HO (high data rate outside), LI (low data rate inside) and LO (low data rate outside) respectively [11]. The main characteristics and requirements of the 4 categories of WAIC are shown in Table 1. Therefore, WAIC system can be defined as: once a system meets these requirements of Table 1, the system can be called a WAIC system.

Through discussion and research, ITU decided to allocate 4200 to 4400 MHz and 22 to 23 GHz as the spectrum of WAIC in World Radio Communication Conferences 2015 (WRC-15) [12]. This spectrum is allocated into ARNS (Aeronautical Radio Navigation Service). And this spectrum is also used by radio altimeter installed on the aircraft.

TABLE 1. Technical Characteristics for WAIC Systems [11].

	Low data rate inside	Low data rate outside	High data rate inside	High data rate outside
Aggregate average data rate of network (kbit/s)	394	856	18,385	12,300
Range of average data rate per link (kbit/s)	0.01-0.8	0.02-8	12.5-1,600	45-1,000
Peak data rate per link (kbit/s)	1	8	4,800	1000
Number of nodes	4,150	400	125	65
Installation domain	Inside	Outside	Inside	Outside
Maximum distance between TX and RX (meter)	15	15	15	15
Typical channel	NLOS	LOS/NLOS	LOS/NLOS	LOS
Application	Sensing and control (cabin temperatures, pressure control, smoke, door)	Sensing and control (temperature, pressure, structural stress, landing gear)	Sensing and communication (engine, avionics data bus, voice/video/image)	Sensing and control (structure, vibration control, voice/video/image)
Most dominant DAL levels	C/D	A/B	B/C	B/C
Spectrum requirements per aircraft (MHz)	35	35	53	53
Maximum transmit power (mW)	10	10	50	50
Receiver sensitivity (dBm)	-91	-91	-77	-77

Developing a WAIC system from scratch is inefficient, so it is generally believed that some modification of existing wireless standards is a more effective way. Ultra-wideband (UWB) communication technology, as one of the optional systems of WAIC, has the advantages of low transmission signal power spectral density, low interception ability [13]. And UWB communication can provide several centimeters of positioning accuracy. Moreover, UWB communication frequency bands specified in the ECMA-368 standard, i.e. 3.1 to 10.6 GHz, meet the WAIC frequency band requirements [14]. In [15], UWB was selected as the most suitable COTS (Commercial Off The Shelf) technology in avionics context. Therefore, our work uses UWB signal as the transmitting signal and UWB channel environment in the aircraft is adopted. Furthermore, the application of cooperative communication technology to WAIC network can increase channel capacity and system reliability [16]. However, cooperative communication leads to an increase in the power density of the system. This may cause electromagnetic interference to other systems with overlapping frequency bands, e.g. ARNS. [17]. Hence, how to reduce the power density of cooperative communication is a challenge for WAIC systems research.

B. RELATED WORK

For the early application of WAIC, US military cooperated with MSSI (Multispectral Solution Inc) company to develop an aircraft wireless communication system based on impulse radio ultra wideband (IR-UWB) in 2003 [18]. The system provides 64 Kb/s voice communication and uses TDMA (Time Division Multiple Access) to accommodate the calls between 8 crew members. The European Union began to implement the Wireless Cabin project from 2013 [19]. Wireless communication technology in the cabin and the wireless interconnection between some equipment outside the cabin are studied. The Aerospace Vehicle Systems Institute (AVSI) has extensively investigated the total spectrum demand to support various WAIC applications and has analyzed the compatibility and interference issue with existing aeronautical radio navigation service below 15.7 GHz [20]. After ITU allocate 4200 to 4400 MHz and 22 to 23 GHz as the spectrum of WAIC in WRC-15, compatibility analysis of WAIC to radio altimeter was studied in [21]. The results of the compatibility present that the interference of the WAIC system is not harmful to the radio altimeter, but the power density of WAIC system should not be too high.

Due to the requirement of low time delay and high data rate in avionics system, UWB is considered to be the most suitable technology for avionics system [22]. ECMA-368 standard defines a kind of media access control layer (MAC) and physical layer standard of UWB wireless communication [23]. A MB-OFDM-UWB wireless avionics intra-communications system based on ECMA-368 standard is designed in [15], [22], [23], and the security and reliability of UWB communication are evaluated and verified. Due to limitations on the transmitter power level, UWB system faces significant design challenges to achieve the desired performance and coverage range. [24] analyzed the optimal cooperative relaying strategies in the MAC layer while considering the UWB unique properties to increase the system throughput. Cooperative communication technology can effectively share transmission resources and form a virtual antenna array by means of resource cooperation between nodes in the network, so as to obtain diversity gain [25].The research works in [26], [27] have proved the significant potential of cooperative diversity in wireless networks. On this basis, [28]–[30] studied the relay selection algorithm based on outage probability under AF protocol, and gave the selection algorithm of optimal relay set under the condition of equal power allocation. Ahmed proposed a cooperative relay selection scheme for

UWB wireless avionics networks based on delay and bit error rate (BER), in which the optimal relay node is selected from a group of potential nodes for data transmission [31]. But he found that the result of cooperative communication is positively correlated with the power of the UWB system. However, due to the limited spectrum resources allocated, excessive power density of WAIC system will affect other systems [21]. Therefore, it is still a challenge to reduce the power density of cooperative relay UWB system while meeting the communication requirements.

C. CONTRIBUTIONS

A power allocation and relay selection scheme is proposed in this article so that the power density of the WAIC network is minimized under the condition of outage probability limitation. The scheme optimizes the power of the source node and each relay node before relay selection. Then the optimal relay selection can be determined only by judging the number of relay nodes selected. Finally redistributes the power between the source node and the optimal relay set. This method avoids the influence of selecting relay nodes under equal power allocation on outage performance, with some statistical knowledge of the UWB channel gains is available to the transmitting nodes. The main contributions of our work are summarized as follows:

- The expressions of outage probability of the mutual information (MI) for AF cooperative communication in WAIC network are derived according to the UWB multi-cluster multipath channel model.
- We formulate a power optimization problem that considers the distance, frequency, and channel model within the channel state information (CSI) under the condition that the outage probability is limited, so that the power density of the WAIC network is minimized.
- A minimum power density based relay selection and power allocation algorithm is proposed, and the optimal set of relay nodes can be obtained according to the power allocation factor sequence of potential relay nodes.
- Numerical results show that the proposed MPRP algorithm produces less power density than the traditional algorithm, which can effectively improve system performance and efficiency and thus the external electromagnetic interference generated by the system is minimized.

D. PAPER ORGANIZATION

The rest of this article is organized as follows. In Section II, a system model of the two-way and multi-relay scheme is described. Then channel model of WAIC is introduced, and the expression of the outage probability is given. Subsequently, Section III formulates the power allocation problem with outage probability constraint and propose MPRP algorithm. Section IV evaluates the outage probability, signal-to-noise ratio and signal power density of the MPRP algorithm. Finally, the conclusions have been provided in Section V.

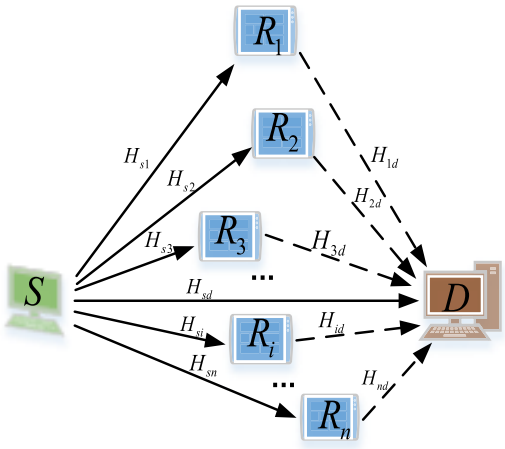

FIGURE 1. WAIC network model with one source node S, one destination node D and n relay nodes R_i ($i = 1, \ldots, n$). The channel gain of $S \rightarrow R_i$, $S \rightarrow D$, $Ri \rightarrow D$ are represented by H_{si}, H_{sd}, H_{id} respectively.

II. SYSTEM MODEL

A. CHANNEL MODEL

We consider a two-hop WAIC relay communication system which consists of one source node S, one destination node D and n relay nodes R_i ($i = 1, \ldots, n$) with amplify and forward (AF) mode as illustrated in Fig. 1. The power transmitted at the source and relay nodes are P_s and P_i. $L = \{1, 2, \ldots, l\}$ denote the collection of relay nodes involved in forwarding data. The channel gain of $S \rightarrow R_i$, $S \rightarrow D$, $Ri \rightarrow D$ are represented by H_{si}, H_{sd}, H_{id} respectively. The MB-OFDM-UWB channels are statistically independent, and obeys frequency flat fading. Due to the multipath effect of in-flight UWB communication, we define the equivalent channel gain H as follows:

$$H = PL(d) \cdot h(t). \tag{1}$$

where $PL(d)$ is the pathloss averaged over the small-scale fading, $h(t)$ is the impulse response in complex baseband. IEEE802.15.3a report [32] describes the pathloss $PL(d)$ in dB as:

$$PL(d) = PL_0 + 10\varepsilon_p \lg(d/d_0) + S. \tag{2}$$

where the reference distance d_0 is set to 1 m, S is a Gaussian-distributed random variable with zero mean and standard deviation σ_S, and PL_0 is the pathloss at the reference distance. ε_p is the pathloss exponent. The pathloss exponent also depends on the environment, and on whether a line-of-sight(LOS) connection exists between the transmitter and receiver or not.

The complex environment inside the aircraft causes multipath effects in signal transmission. The process of forming multi-path and multi-cluster channels is shown in the Fig. 2.

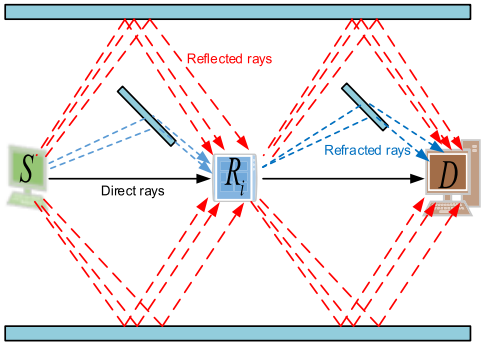

FIGURE 2. The process of forming multi-path and multi-cluster channels. There are three types of rays: direct rays, reflected rays and refracted rays. So there are multi-path effects on R_i and D nodes.

Thus, the impulse response $h(t)$ is described as follows:

$$h(t) = \sum_{l=0}^{L} \sum_{k=0}^{K} \alpha_{k,l} \delta(t - T_l - \tau_{k,l}). \tag{3}$$

where T_l denotes time delay of l-th cluster. T_l can be represented by Poisson distribution:

$$p(T_l \,|T_{l-1}) = \Lambda e^{-\Lambda(T_l - T_{l-1})} \qquad l > 0. \tag{4}$$

Λ is the cluster arrival rate. In Eq. 3, $\tau_{k,l}$ is the time delay of the k-th ray in the l-th cluster, which also can be represented by Poisson distribution:

$$p(\tau_{k,l} \,|\tau_{(k-1),l}) = \lambda e^{-\lambda(\tau_{k,l} - \tau_{(k-1),l})} k > 0. \tag{5}$$

where λ is the ray arrival rate. $\alpha_{k,l}$ is amplitude gain coefficient of the k-th ray in the l-th cluster, which can be expressed as:

$$\alpha_{k,l} = p_{k,l} \beta_{k,l}. \tag{6}$$

$p_{k,l}$ is equal probability of +1 or -1, $\beta_{k,l}$ denotes the channel coefficient of the k-th ray in the l-th cluster and obeys logarithmic distribution:

$$\beta_{k,l} = 10^{x_{k,l}/20}. \tag{7}$$

$x_{k,l}$ is Gaussian random variable with the mean value $\mu_{k,l}$ and variance $\sigma_{k,l}^2$. And $x_{k,l}$ can be expressed as:

$$x_{k,l} = \mu_{k,l} + \xi_l + \zeta_{k,l}. \tag{8}$$

Gaussian random variables ξ_l and $\zeta_{k,l}$ represent the channel coefficient variation of the cluster and ray. Assuming σ_ξ^2 and σ_ζ^2 the variance of ξ_l and $\zeta_{k,l}$. Since the energy of both clusters and rays obey exponential decay, the following formula is obtained:

$$\begin{aligned} \left|\beta_{k,l}\right|^2 &= \left| 10^{\frac{\mu_{k,l} + \xi_l + \zeta_{k,l}}{20}} \right|^2 \\ &= \left|\beta_{0,0}\right|^2 e^{\frac{-T_l}{\Gamma}} e^{\frac{-\tau_{k,l}}{\omega}}, \end{aligned} \tag{9}$$

TABLE 2. Notations.

Parameter	Description
TX	Transmitter
RX	Receiver
LOS	Line of sight
NLOS	Not line of sight
DAL	Development assurance level (A to E)
SNR	Signal noise ratio
S	Source node
D	Destination node
R_i	i -th relay node
P_v	Power transmitted at node v
H_{vw}	The channel gain of node v to w
$PL(d)$	Pathloss averaged over the small-scale fading
T_l	Time delay of $l-$th cluster
Λ	Cluster arrival rate
$\tau_{k,l}$	Time delay of the $k-$th ray in the $l-$th cluster
λ	Ray arrival rate
$\alpha_{k,l}$	Amplitude gain coefficient of the $k-$th ray in the $l-$th cluster
Γ	Cluster attenuation coefficient
ω	Ray attenuation coefficient
$h(t)$	Impulse response in complex baseband
I	Mutual Information
P_{out}	Outage probability
P_{outMax}	Maximum allowable outage probability of the system
ρ	Equivalent power density
W	Frequency range of transmitting
β_v	power allocation factor of node v
$\mathbf{R}_i$	Selected i relay nodes sequence
$\mathbf{B}_i$	Sequence of power allocation factors for source node and i relay nodes

$$\mu_{k,l} = \frac{10 \ln\left(\left|\beta_{0,0}\right|^2\right) - 10\frac{T_l}{\Gamma} - 10 \ln \frac{\tau_{k,l}}{\omega}}{\ln 10} - \frac{\left(\sigma_\xi^2 + \sigma_\zeta^2\right) \ln 10}{20}. \tag{10}$$

where Γ is the cluster attenuation coefficient, ω is the ray attenuation coefficient. Then we get that H_{si}, H_{sd}, H_{id} obey the characteristic of equivalent channel gain H.

B. TRANSMISSION MODEL

The cooperative communication process is divided into two stages. In the first stage, the source node broadcasts the data it needs to send, and the selected relay node and destination node receive the data from the source node at the same time. Let the data sent by the source node be x. z_{sd} and z_{si} represent additive white Gaussian noise (AGWN) on the corresponding channel, respectively. They are independent complex Gaussian random variables with mean value of zero and variance of Z_{sd} and Z_{si}. The system uses MB-OFDM-UWB signal as the transmitting signal, then all channels are orthogonal in frequency to avoid mutual interference between channels. The details of the transmitter and receiver are shown in Fig. 3.

The data received by destination node D and relay node R_i participating in cooperation are as follows:

$$y_{sd} = H_{sd}\sqrt{P_s}x + z_{sd}, \tag{11}$$

$$rCly_{si} = H_{si}\sqrt{P_s}x + z_{si}, i \in L. \tag{12}$$

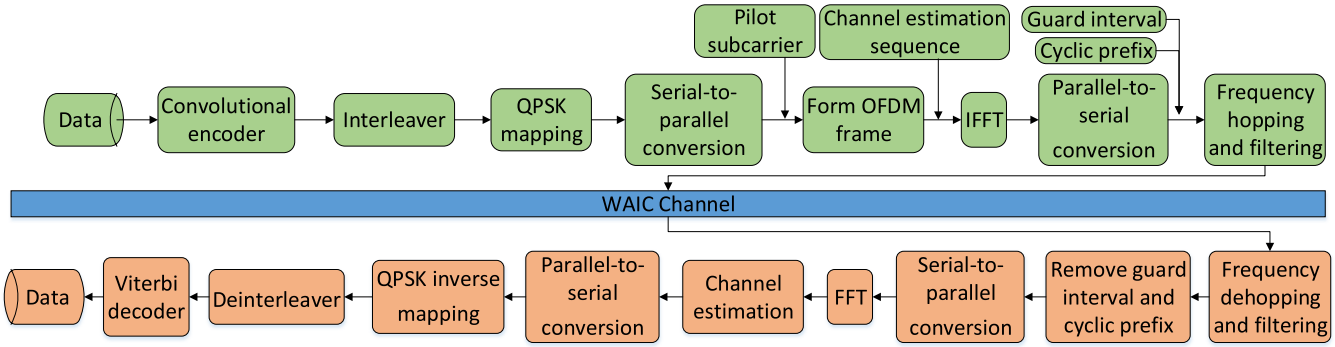

FIGURE 3. Schematic diagram of transmitter and receiver. The transmitter includes convolutional encoder, QPSK (Quadrature Phase Shift Keying) mapping module, IFFT (Invert Fast Fourier Transformation) module, frequency hopping module, etc. The receiver includes FFT (Fast Fourier Transformation) module, QPSK inverse mapping module Viterbi decoder, etc.

In the second stage, the relay node will receive the data and then amplified and forwarded to the destination node. The data forwarded by the relay node are $x_i = \alpha y_{si}$, where

$$\alpha = \frac{1}{\sqrt{P_s|H_{si}|^2 + {z_{si}}^2}}, \tag{13}$$

is the scaling factor [25]. Then data received by the destination node from relay node R_i can be expressed as follows:

$$y_{id} = H_{id}\sqrt{P_i}x_i + z_{id}, i \in L. \tag{14}$$

where z_{id} is AGWN signal, which is independent complex Gaussian random variable with zero mean value and Z_{id} variance. For convenience of consideration,let $Z_{si} = Z_{id} = Z_{sd} = Z_0$.

C. OUTAGE PROBABILITY MODEL

Assuming that all relay nodes participate in cooperation under AF protocol. Because the data from the source node through n relay nodes to the destination node, there are $n+1$ time slots. Therefore, the Mutual Information (MI) [33] from the source node to the destination node can be expressed as:

$$I = \frac{1}{n+1}\log_2\left[1 + \frac{P_s|H_{sd}|^2}{Z_0} + \sum_{i=1}^{n} f\left(\frac{P_s|H_{si}|^2}{Z_0}, \frac{P_i|H_{id}|^2}{Z_0}\right)\right]. \tag{15}$$

In this formula, the fraction $1/(n+1)$ means that the source uses only $1/(n+1)$ of the total bandwidth, and

$$f(x, y) = \frac{xy}{x + y + 1}. \tag{16}$$

The received SNR at the destination node are all proportional to $1/Z_0$. Hence denoting $1/Z_0 = \gamma$ serves as the equivalent SNR. Then, the outage event will occur when the MI could not meet the required user rate.

Theorem 1: Let the required rate be R in bits/time slot. Thus the outage probability is defined as:

$$\begin{aligned} P_{out} &= \Pr[I < R] \\ &= \Pr\left[\frac{1}{n+1}\log_2\left(1 + \frac{P_s|H_{sd}|^2}{Z_0} + \sum_{i=1}^{n} f\left(\frac{P_s|H_{si}|^2}{Z_0}, \frac{P_i|H_{id}|^2}{Z_0}\right)\right) < R\right] \\ &= \Pr\left[P_s|H_{sd}|^2\gamma + \sum_{i=1}^{n} f\left(P_s|H_{si}|^2\gamma, P_i|H_{id}|^2\gamma\right) < 2^{(n+1)R} - 1\right] \\ &\approx \frac{\left(\left(2^{(n+1)R} - 1\right)Z_0\right)^{n+1}}{P_s\sigma_{s,d}^2 M_{sd}^2 (n+1)} \cdot \prod_{i=1}^{n}\left(\frac{1}{P_s\sigma_{s,i}^2 M_{si}^2} + \frac{1}{P_i\sigma_{i,d}^2 M_{id}^2}\right). \end{aligned} \tag{17}$$

where $\Pr[\cdot]$ means the probability of the formula, M_{sd}, M_{si}, and M_{id} are variables computed by parameters related to H_{sd}, H_{si}, and H_{id} respectively. The detailed expression of M_{sd}, M_{si}, M_{id} is shown in the proof.

Proof: : The channel gain of WAIC takes into account the influence of multi-cluster and multi-path. And the later the cluster arrives in the same impulse response, the smaller the amplitude. Thus the expression of impulse response $h(t)$ can be simplified as follows:

$$\begin{aligned} h(t) &= \sum_{l=0}^{L}\sum_{k=0}^{K}\alpha_{k,l}\delta(t - T_l - \tau_{k,l}) \\ &\approx \sum_{l=0}^{L} x_l\delta(t - T_l{}') \\ &= x_1\delta(t - T_1{}') + x_2\delta(t - T_2{}') \\ &\quad + \ldots + x_L\delta(t - T_L{}') \\ &\approx x_1\delta(t - T_1{}') + x_2\delta(t - T_2{}') + x_3\delta(t - T_3{}'). \end{aligned} \tag{18}$$

where x_l and $T_l{}'$ represent the combined amplitude and time delay of $l-th$ cluster. Without affecting the result of relay selection algorithm, these two variables can be calculated from the following equations:

$$x_l = \sum_{k=0}^{K} \frac{\alpha_{k,l}}{K}, \tag{19}$$

$$T_l{}' = T_l + \frac{\tau_{K,l}}{2}. \tag{20}$$

In the calculation, T_l can be used to replace $T_l{}'$ approximately, which has no effect on the result of relay selection algorithm. The outage probability is

$$\begin{aligned} P_{out} &= \Pr[I < R] \\ &= \Pr\left[\frac{1}{n+1}\log_2\left(1+\frac{P_s|H_{sd}|^2}{Z_0} \right.\right. \\ &\quad \left.\left. +\sum_{i=1}^{n} f\left(\frac{P_s|H_{si}|^2}{Z_0}, \frac{P_i|H_{id}|^2}{Z_0}\right)\right) < R\right] \\ &= \Pr\left[\frac{P_s|H_{sd}|^2}{Z_0} + \sum_{i=1}^{n} f\left(\frac{P_s|H_{si}|^2}{Z_0}, \frac{P_i|H_{id}|^2}{Z_0}\right) \right. \\ &\quad \left. < 2^{(n+1)R} - 1\right]. \end{aligned} \tag{21}$$

Since

$$\begin{aligned} \sum_{i=1}^{n} f\left(P_s|H_{si}|^2\gamma, P_i|H_{id}|^2\gamma\right) &= \sum_{i=1}^{n} \frac{P_s|H_{si}|^2\gamma \cdot P_i|H_{id}|^2\gamma}{1+P_s|H_{si}|^2\gamma+P_i|H_{id}|^2\gamma} \\ &> \max_i \frac{P_s|H_{si}|^2\gamma \cdot P_i|H_{id}|^2\gamma}{1+P_s|H_{si}|^2\gamma+P_i|H_{id}|^2\gamma}. \end{aligned} \tag{22}$$

Denote $P_s|H_{sd}|^2/Z_0 = a_0$, $P_s|H_{si}|^2/Z_0 = a_i$, $P_i|H_{id}|^2/Z_0 = b_i$. Following the approach of [34], we can introduce an upper bound for P_{out} as:

$$\begin{aligned} \overline{P_{out}} &= \Pr\left[\frac{1}{n+1}\log_2\left(1+a_0+\max_i \frac{a_i \cdot b_i}{1+a_i+b_i}\right) < R\right] \\ &= \Pr\left[\max_i \frac{a_i \cdot b_i}{1+a_i+b_i} < 2^{(n+1)R} - 1 - a_0\right]. \end{aligned} \tag{23}$$

From Eq. 1, Eq. 2 and Eq. 18, we can get

$$\begin{aligned} |H_{sd}|^2 &= |PL_{sd}(d) \cdot h_{sd}(t)|^2 \\ &= \left|PL_{sd}(d)\left(x_{sd\,1}\delta(t-T_{sd\,1}{}') + x_{sd\,2}\delta(t-T_{sd\,2}{}')\right.\right. \\ &\quad \left.\left. +x_{sd\,3}\delta(t-T_{sd\,3}{}')\right)\right|^2. \end{aligned} \tag{24}$$

where $x_{sd\,1}\delta(t-T_{sd}{}'_1)+x_{sd\,2}\delta(t-T_{sd}{}'_2)+x_{sd\,3}\delta(t-T_{sd}{}'_3)$ can be regarded as the three peaks that arrive successively. Then $|PL_{sd}(d)\,h_{sd}(t)|$ can be equal to the maximum merge ratio operation of $|PL_{sd}(d)|$ with coefficients of $x_{sd\,1}, x_{sd\,2}, x_{sd\,3}$:

$$|PL_{sd}(d)\,h_{sd}(t)| = |PL_{sd}(d)|\,M_{sd}. \tag{25}$$

where

$$M_{sd} = \frac{x_{sd\,1}x_{sd\,2}x_{sd\,3}}{x_{sd\,1}+x_{sd\,2}+x_{sd\,3}}. \tag{26}$$

Thus,

$$a_0 \cdot Z_0 = P_s|H_{sd}|^2 = P_s|PL_{sd}(d)|^2 M_{sd}^2, \tag{27}$$

is exponentially distributed variable with parameter λ_0. Where

$$\lambda_0 = \frac{1}{P_s\sigma_{s,d}^2 M_{sd}^2}. \tag{28}$$

Denote $2^{(n+1)R} - 1$ with v, then we can transform the $\overline{P_{out}}$ as follows:

$$\begin{aligned} \overline{P_{out}} &= \Pr\left[\max_i \frac{a_i \cdot b_i \cdot Z_0}{1+a_i+b_i} < vZ_0 - a_0Z_0\right] \\ &= \int_0^{vZ_0} \Pr\left[\max_i \frac{a_i \cdot b_i \cdot Z_0}{1+a_i+b_i} < vZ_0 - x\right]\lambda_0 e^{-\lambda_0 x}dx \\ &= \int_0^1 \Pr\left[\max_i \frac{a_i \cdot b_i}{1+a_i+b_i} < vx'\right]vZ_0\lambda_0 e^{-\lambda_0 vZ_0(1-x')}dx' \\ &= \int_0^1 \left(\prod_{i=1}^{n} \Pr\left[\frac{a_i \cdot b_i}{1+a_i+b_i} < vx'\right]\right)vZ_0\lambda_0 e^{-\lambda_0 vZ_0(1-x')}dx' \\ &= (vZ_0)^{n+1}\lambda_0 \int_0^1 \left(\prod_{i=1}^{n} \frac{\Pr\left[\frac{a_i \cdot b_i}{1+a_i+b_i} < vx'\right]}{vZ_0x'}\right) \\ &\quad \cdot (x')^m e^{-\lambda_0 vZ_0(1-x')}dx'. \end{aligned} \tag{29}$$

Using $x' = 1 - x/(vZ_0)$. According to [35], the SNR is almost 20 dB when the bit error rate is lower than 10^{-5}. Thus it can be assumed that $vZ_0 \to 0$ because $\gamma = 1/Z_0$ is the equivalent SNR. Then Eq. 29 can be transformed into the following form:

$$\overline{P_{out}} = (vZ_0)^{n+1}\lambda_0 \int_0^1 \left(\prod_{i=1}^{n} \frac{\Pr\left[\frac{a_i \cdot b_i}{1+a_i+b_i} < vx'\right]}{vZ_0x'}\right)(x')^m dx'. \tag{30}$$

By Lemma 1 in Appendix 1 of [25], the following equation can be obtained:

$$\frac{1}{vZ_0x'}\Pr\left[\frac{a_i \cdot b_i}{1+a_i+b_i} < vx'\right] \approx \lambda_i + \kappa_i. \tag{31}$$

where λ_i and κ_i are the exponential distribution parameters of $P_s|H_{si}|^2$ and $P_i|H_{id}|^2$ respectively:

$$\lambda_i = \frac{1}{P_s\sigma_{s,i}^2 M_{si}^2}, \kappa_i = \frac{1}{P_i\sigma_{i,d}^2 M_{id}^2}. \tag{32}$$

where M_{si} and M_{id} are obtained by the same process as Eq. 26:

$$M_{si} = \frac{x_{si\,1}x_{si\,2}x_{si\,3}}{x_{si\,1}+x_{si\,2}+x_{si\,3}}, M_{id} = \frac{x_{si\,1}x_{si\,2}x_{si\,3}}{x_{si\,1}+x_{si\,2}+x_{si\,3}}. \tag{33}$$

And in this algorithm, P_{out} can be replaced by $\overline{P_{out}}$ approximately without affecting the relay selection result [25]. Therefore, we can get the expression of P_{out} from Eq. 30

and Eq. 31 as follows:

$$\begin{aligned} P_{out} &\approx \overline{P_{out}} \\ &= (vZ_0)^{n+1}\lambda_0 \int_0^1 \left(\prod_{i=1}^{n}\lambda_i + \kappa_i\right)(x')^m dx' \\ &= \frac{(vZ_0)^{n+1}\lambda_0}{n+1}\prod_{i=1}^{n}(\lambda_i+\kappa_i). \end{aligned} \tag{34}$$

Theorem 1 is proved.

III. MINIMUM POWER DENSITY BASED RELAY SELECTION AND POWER ALLOCATION (MPRP) ALGORITHM

A. POWER ALLOCATION STRATEGY

Outage probability is an important evaluation standard of system communication quality in cooperative communication [33]. On this basis, some constraints in practical cooperative communication are considered. Therefore, we studies the optimal power allocation factor of source node and potential relay node to minimize power density under the condition of outage probability. For the convenience of calculation, we can define $\rho = P_{all}/W$ as the equivalent power density, where P_{all} is the total system power and W is the frequency range of the system. Thus, the problem can be described by the following mathematical model:

$$\begin{aligned} &\min \rho = \frac{P_s + \sum_{i=1}^{n} P_i}{W}, \\ &s.t. P_{out} \le P_{outMax}. \end{aligned} \tag{35}$$

where P_{outMax} is the maximum allowable outage probability of the system. It is assumed that the power allocation factor of the source node and relay nodes are β_0 and β_i, $i = 1, \ldots, n$, then:

$$P_s = \beta_0 \rho W, \tag{36}$$

$$P_i = \beta_i \rho W. \tag{37}$$

And the constraint condition $\sum_{i=0}^{n}\beta_i = 1$ is satisfied. Denote $M_{sd}\sigma_{s,d}$, $M_{si}\sigma_{s,i}$, $M_{id}\sigma_{i,d}$ with $\psi_{s,d}$, $\psi_{s,i}$, $\psi_{i,d}$ respectively. Then the average outage probability of Eq. 17 can be expressed as:

$$\begin{aligned} P_{out} &= \frac{\lambda_0\left(\left(2^{(n+1)R}-1\right)Z_0\right)^{n+1}\prod_{i=1}^{n}(\lambda_i+\kappa_i)}{n+1} \\ &= \frac{\left(\left(2^{(n+1)R}-1\right)Z_0\right)^{n+1}}{(n+1)\,\beta_0\rho W\psi_{s,d}^2}\prod_{i=1}^{n}\left(\frac{1}{\beta_0\rho W\psi_{s,i}^2}+\frac{1}{\beta_i\rho W\psi_{i,d}^2}\right) \\ \Leftrightarrow \\ \rho^{n+1} &= \frac{\left(\left(2^{(n+1)R}-1\right)Z_0\right)^{n+1}}{(n+1)\,P_{out}\beta_0\psi_{s,d}^2 W^{n+1}}\prod_{i=1}^{n}\left(\frac{1}{\beta_0\psi_{s,i}^2}+\frac{1}{\beta_i\psi_{i,d}^2}\right). \end{aligned} \tag{38}$$

Denote $\left(\left(2^{(n+1)R}-1\right)Z_0\right)^{n+1}/(n+1)\,P_{out}\psi_{s,d}^2 W^{n+1}$ with M, and then Eq. 38 can be transformed into the following form:

$$\begin{aligned} \rho^{n+1} &= \frac{M}{\beta_0}\prod_{i=1}^{n}\left(\frac{1}{\beta_0\psi_{s,i}^2}+\frac{1}{\beta_i\psi_{i,d}^2}\right) \\ &\Leftrightarrow \\ (n+1)\log\rho &= \sum_{i=1}^{n}\log\left(\beta_i\psi_{i,d}^2+\beta_0\psi_{s,i}^2\right) \\ &\quad -\sum_{i=1}^{n}\log\left(\psi_{s,i}^2\beta_i\psi_{i,d}^2\right)-\log\beta_0+\log M. \end{aligned} \tag{39}$$

The last term in the Eq. 39 is a constant when the WAIC environment is determined, which has no effect on the optimization result and can be ignored. This is a typical convex optimization problem which can be solved by classical Lagrange multiplier method [30]. The Lagrange cost function is defined as:

$$\begin{aligned} L(\beta_0, \beta_i) = &\sum_{i=1}^{n}\log\left(\beta_i\psi_{i,d}^2+\beta_0\psi_{s,i}^2\right)-\sum_{i=1}^{n}\log\left(\psi_{s,i}^2\beta_i\psi_{i,d}^2\right) \\ &-\log\beta_0+\lambda\left(\sum_{i=1}^{n}\beta_i-1\right), \end{aligned} \tag{40}$$

while λ is the Lagrange multiplier. Take the derivative of β_0, β_i, λ respectively:

$$\frac{\partial L}{\partial\beta_0} = \sum_{i=1}^{n}\frac{\psi_{si}^2}{\beta_0\psi_{si}^2+\beta_i\psi_{id}^2}-\frac{1}{\beta_0}+\lambda, \tag{41}$$

$$\frac{\partial L}{\partial\beta_i} = \frac{\psi_{id}^2}{\beta_0\psi_{si}^2+\beta_i\psi_{id}^2}-\frac{1}{\beta_i}+\lambda, i=1,\ldots n, \tag{42}$$

$$\frac{\partial L}{\partial\lambda} = \sum_{i=0}^{n}\beta_i - 1. \tag{43}$$

Denote

$$x = (\beta_0, \beta_1, \ldots \beta_n, \lambda). \tag{44}$$

And

$$F(x) = \left(\frac{\partial L}{\partial\beta_0}, \frac{\partial L}{\partial\beta_1}, \ldots \frac{\partial L}{\partial\beta_n}, \frac{\partial L}{\partial\lambda}\right) = 0. \tag{45}$$

Eq. 45 is a typical problem of solving nonlinear systems.

Lemma 1: : By using the Quasi-Newton method for nonlinear systems [36], the power allocation factor of the source node and all potential relay nodes can be obtained as

$$\begin{aligned} \beta_0^{(j+1)} = \beta_0^{(j)} - \Bigg(&a_{11}^{(j)}\left(\frac{\partial L}{\partial\beta_0}\right)^{(j)} + \sum_{m=1}^{n}a_{1(m+1)}^{(j)}\left(\frac{\partial L}{\partial\beta_m}\right)^{(j)} \\ &+ a_{1(n+2)}^{(j)}\left(\frac{\partial L}{\partial\lambda}\right)^{(j)}\Bigg), \end{aligned} \tag{46}$$

$$\beta_i^{(j+1)} = \beta_i^{(j)} - \left(a_{(i+1)1}^{(j)} \left(\frac{\partial L}{\partial \beta_0} \right)^{(j)} + \sum_{m=1}^{n} a_{(i+1)(m+1)}^{(j)} \left(\frac{\partial L}{\partial \beta_m} \right)^{(j)} + a_{(i+1)(n+2)}^{(j)} \left(\frac{\partial L}{\partial \lambda} \right)^{(j)} \right), i = 1, 2 \ldots n. \quad (47)$$

While j and a_{mn}^{j} is the number of iterations and elements in iteration matrix at Quasi-Newton method respectively.

Proof: : The Newton's method for nonlinear systems is shown as follows:

$$x^{(j)} = x^{(j-1)} - F'\left(x^{(j-1)}\right)^{-1} F\left(x^{(j-1)}\right). \quad (48)$$

According to the description in [36], iteration matrix A_1 can be defined as an approximate substitute for $F'\left(x^{(1)}\right)$ in Quasi-Newton Method:

$$A_1 = F'\left(x^{(0)}\right) + \frac{\left[F\left(x^{(1)}\right) - F\left(x^{(0)}\right) - F'\left(x^{(0)}\right)\left(x^{(1)} - x^{(0)}\right)\right]}{\left\|x^{(1)} - x^{(0)}\right\|_2^2} \cdot \left(x^{(1)} - x^{(0)}\right)^T. \quad (49)$$

Then $x^{(2)} = x^{(1)} - A_1^{-1} F\left(x^{(1)}\right)$ is determined. In general, once $x^{(j)}$ has been determined, $x^{(j+1)}$ is computed by

$$A_j = A_{j-1} + \frac{\left[F\left(x^{(j)}\right) - F\left(x^{(j-1)}\right) - A_{j-1}\left(x^{(j)} - x^{(j-1)}\right)\right]}{\left\|x^{(j)} - x^{(j-1)}\right\|_2^2} \cdot \left(x^{(j)} - x^{(j-1)}\right)^T, \quad (50)$$

and

$$x^{(j+1)} = x^{(j)} - A_j^{-1} F\left(x^{(j)}\right). \quad (51)$$

Take Eq. 41 to Eq. 45 into Eq. 51. Thus,

$$\beta_0^{(j+1)} = \beta_0^{(j)} - \left(a_{11}^{(j)} \left(\frac{\partial L}{\partial \beta_0} \right)^{(j)} + \sum_{m=1}^{n} a_{1(m+1)}^{(j)} \left(\frac{\partial L}{\partial \beta_m} \right)^{(j)} + a_{1(n+2)}^{(j)} \left(\frac{\partial L}{\partial \lambda} \right)^{(j)} \right), \quad (52)$$

$$\beta_i^{(j+1)} = \beta_i^{(j)} - \left(a_{(i+1)1}^{(j)} \left(\frac{\partial L}{\partial \beta_0} \right)^{(j)} + \sum_{m=1}^{n} a_{(i+1)(m+1)}^{(j)} \left(\frac{\partial L}{\partial \beta_m} \right)^{(j)} + a_{(i+1)(n+2)}^{(j)} \left(\frac{\partial L}{\partial \lambda} \right)^{(j)} \right), i = 1, 2 \ldots n, \quad (53)$$

$$\lambda^{(j+1)} = \lambda^{(j)} - \left(a_{(n+2)1}^{(j)} \left(\frac{\partial L}{\partial \beta_0} \right)^{(j)} + \sum_{m=1}^{n} a_{(n+2)(m+1)}^{(j)} \left(\frac{\partial L}{\partial \beta_m} \right)^{(j)} + a_{(n+2)(n+2)}^{(j)} \left(\frac{\partial L}{\partial \lambda} \right)^{(j)} \right). \quad (54)$$

Lemma 1 is proved.

B. RELAY SELECTION STRATEGY

Avionics system attaches great importance to low delay performance, so the computational complexity should be reduced as much as possible to avoid bringing too high processing delay to the system. Therefore, the traditional exhaustive algorithm, which calculates all possible permutations and combinations of relay nodes one by one, is not suitable for WAIC system. In order to solve the problem of high processing delay caused by too much calculation. A low complexity relay selection algorithm is proposed in this section. After obtaining the allocation factors of all potential relay nodes, the optimal relay selection with minimum power density can be obtained by determining how many nodes really participate in the relay process.

Let $B = \{\beta_0, \beta_{sq1}, \beta_{sq2}, \ldots \beta_{sqn}\}$ represent the sequence of power allocation factors for source node and potential relay nodes, where $\beta_{sq1} > \beta_{sq2} > \ldots > \beta_{sqn}$. Note that β_0 does not participate in sorting.

Theorem 2: : If there are k relay nodes in the optimal relay selection scheme, the power allocation factor of these nodes must be the first k in sequence B.

Proof: : Let $B_1 = \{b_0, b_1, b_2, \ldots b_n\}$ be the power allocation factor sequence obtained by the power allocation algorithm in the previous section and the corresponding relay nodes are $R_1 = \{S, R_1, R_2, \ldots R_n\}$, where $b_1 > b_2 > \ldots > b_n$. Then according to Eq. 35 and Eq. 39, the following formula holds:

$$(n+1)\log\rho_1 = \sum_{i=1}^{n} \log\left(b_i\psi_{i,d}^2 + b_0\psi_{s,i}^2\right) - \sum_{i=1}^{n} \log\left(\psi_{s,i}^2 b_i \psi_{i,d}^2\right) - \log b_0 + \log M_1. \quad (55)$$

where

$$M_1 = \frac{\left(\left(2^{(n+1)R} - 1\right) Z_0\right)^{n+1}}{(n+1)\, P_{out}\, \psi_{s,d}^2\, W^{n+1}}, \quad (56)$$

is a constant when the system state is fixed value. And ρ_1 is the minimum power density that satisfies the outage probability condition Eq. 35 when there are n relay nodes. Let $B_2 = \{c_0, c_1, c_2, \ldots c_{n-1}\}$ and $B_3 = \{d_0, d_1, d_2, \ldots d_{n-2}, d_n\}$ be the power allocation factor sequence for the nodes sequence $R_2 = \{S, R_1, R_2, \ldots R_{n-1}\}$ and $R_3 = \{S, R_1, R_2, \ldots R_{n-2}, R_n\}$. Where B_2 and B_3 satisfies the constraint condition Eq. 35. Then we can get

$$n\log\rho_2 = \sum_{i=1}^{n-1} \log\left(c_i\psi_{i,d}^2 + c_0\psi_{s,i}^2\right) - \sum_{i=1}^{n-1} \log\left(\psi_{s,i}^2 c_i \psi_{i,d}^2\right) - \log c_0 + \log M_2, \quad (57)$$

$$n\log\rho_3 = \sum_{i=1, i\neq n-1}^{n} \log\left(d_i\psi_{i,d}^2 + d_0\psi_{s,i}^2\right) - \log d_0 + \log M_3 - \sum_{i=1, i\neq n-1}^{n} \log\left(\psi_{s,i}^2 d_i \psi_{i,d}^2\right). \quad (58)$$

where ρ_2, ρ_3 are minimum power density when outage probability reach P_{outMax} for R_2, R_3 respectively. And

$$M_2 = M_3 = \frac{\left(\left(2^{nR}-1\right)Z_0\right)^n}{nP_{out}\psi_{s,d}^2 W^n}. \tag{59}$$

According to Eq. 55 to Eq. 59, we have

$$\begin{aligned} & n\log\rho_2 - n\log\rho_3 \\ &= \sum_{i=1}^{n-1}\log\left(c_i\psi_{i,d}^2 + c_0\psi_{s,i}^2\right) - \sum_{i=1,i\neq n-1}^{n}\log\left(d_i\psi_{i,d}^2 + d_0\psi_{s,i}^2\right) \\ &\quad - \sum_{i=1}^{n-1}\log\left(\psi_{s,i}^2 c_i\psi_{i,d}^2\right) + \sum_{i=1,i\neq n-1}^{n}\log\left(\psi_{s,i}^2 d_i\psi_{i,d}^2\right) \\ &\quad - \log c_0 + \log d_0. \end{aligned} \tag{60}$$

Thus the proposition is transformed to prove $\rho_2 < \rho_3$. Change the right side of Eq. 60 as follows:

$$\begin{aligned} & -\Big(\sum_{i=1,i\neq n-1}^{n}\log\left(d_i\psi_{i,d}^2 + d_0\psi_{s,i}^2\right) \\ &\quad + \log\left(b_{n-1}\psi_{n-1,d}^2 + b_0\psi_{s,n-1}^2\right) \\ &\quad - \log d_0 - \log b_0 - \sum_{i=1,i\neq n-1}^{n}\log d_i - \log b_{n-1} \\ &\quad - (n+1)\log\rho_1 + M_1\Big) \\ &\quad + \sum_{i=1}^{n-1}\log\left(c_i\psi_{i,d}^2 + c_0\psi_{s,i}^2\right) - \log c_0 - \sum_{i=1}^{n-1}\log c_i \\ &\quad + \sum_{i=1,i\neq n-1}^{n}\log\left(\psi_{s,i}^2\psi_{i,d}^2\right) \\ &\quad - \sum_{i=1}^{n-1}\log\left(\psi_{s,i}^2\psi_{i,d}^2\right) + \log\left(b_{n-1}\psi_{n-1,d}^2 + b_0\psi_{s,n-1}^2\right) \\ &\quad - \log b_0 \\ &\quad - \log b_{n-1} - (n+1)\log(\rho_1 W) + M_1. \end{aligned} \tag{61}$$

When the power density and power factor sequence are ρ_1 and B_1, the outage probability reaches boundary value P_{outMax}. Thus,

$$\begin{aligned} & -\sum_{i=1,i\neq n-1}^{n}\log\left(d_i\psi_{i,d}^2 + d_0\psi_{s,i}^2\right) - \log\left(b_{n-1}\psi_{n-1,d}^2 + b_0\psi_{s,n-1}^2\right) \\ & + \log d_0 + \log b_0 + \sum_{i=1,i\neq n-1}^{n}\log d_i + \log b_{n-1} - (n+1)\log\rho_1 + M_1 \\ & > P_{outMax}, \end{aligned} \tag{62}$$

in Eq. 61 can be regarded as the outage probability of another power factor sequence when the power density is ρ_1. Then, we can get

$$\begin{aligned} & n\log\rho_2 - n\log\rho_3 \\ & < \sum_{i=1}^{n-1}\log\left(c_i\psi_{i,d}^2 + c_0\psi_{s,i}^2\right) - \log c_0 + \sum_{i=1,i\neq n-1}^{n}\log\left(\psi_{s,i}^2\psi_{i,d}^2\right) \end{aligned}$$

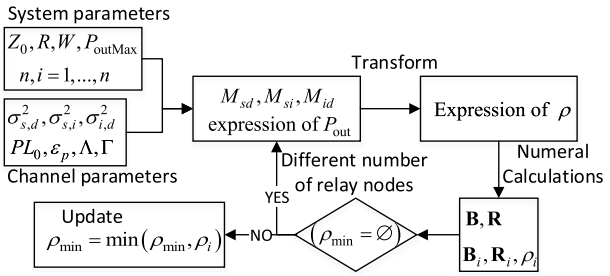

FIGURE 4. Diagram of the proposed MPRP. Expression of outage probability P_{out} is derived based on input system and channel parameters. Then the expression of power density ρ is converted. B_i, R_i and ρ_i are obtained by numerical calculation. Then the $\rho_{\min}$ is obtained by comparing each ρ_i.

$$\begin{aligned} & -\sum_{i=1}^{n-1}\log c_i - \sum_{i=1}^{n-1}\log\left(\psi_{s,i}^2\psi_{i,d}^2\right) + \log\left(b_{n-1}\psi_{n-1,d}^2 + b_0\psi_{s,n-1}^2\right) \\ & - \log b_0 - \log b_{n-1} - (n+1)\log(\rho_1 W) + M_1 - P_{outMax} \\ & < n\log\rho_1 - M_1 + \sum_{i=1,i\neq n-1}^{n}\log\left(\psi_{s,i}^2\psi_{i,d}^2\right) - \sum_{i=1}^{n-1}\log\left(\psi_{s,i}^2\psi_{i,d}^2\right) \\ & - (n+1)\log\rho_1 + M_1 < 0. \end{aligned} \tag{63}$$

Theorem 2 is proved.

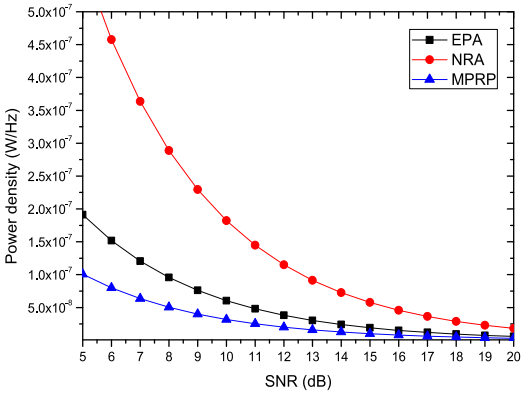

FIGURE 5. The effect of varying the SNR on the power density in EPA, NRA and MPRP. Horizontal coordinates SNR, vertical coordinates for power density. With higher SNR in the network, a good channel environment makes signal transmission easier and ultimately reduces the power density ρ required for all research methods to achieve P_{outMax}. The power density required by the MPRP algorithm is lower.

Therefore, after knowing the power allocation factors of all potential relay nodes, the optimal relay selection can be obtained by determining the number of nodes actually participating in the relay. Denote $R = \{S, R_{sq1}, R_{sq2}, \ldots R_{sqn}\}$ with the node sequence corresponding to the power allocation factors sequence $B = \{\beta_0, \beta_{sq1}, \beta_{sq2}, \ldots \beta_{sqn}\}$. Then the optimal relay selection is only occurs in the following $n+1$ situations:

$$\begin{aligned} & R_0 = \{S, R_{sq1}, R_{sq2}, \ldots R_{sqn}\}, \\ & R_1 = \{S, R_{sq1}, R_{sq2}, \ldots R_{sq(n-1)}\}, \\ & \ldots \\ & R_{n-1} = \{S, R_{sq1}\}, \\ & R_n = \{S\}. \end{aligned} \tag{64}$$

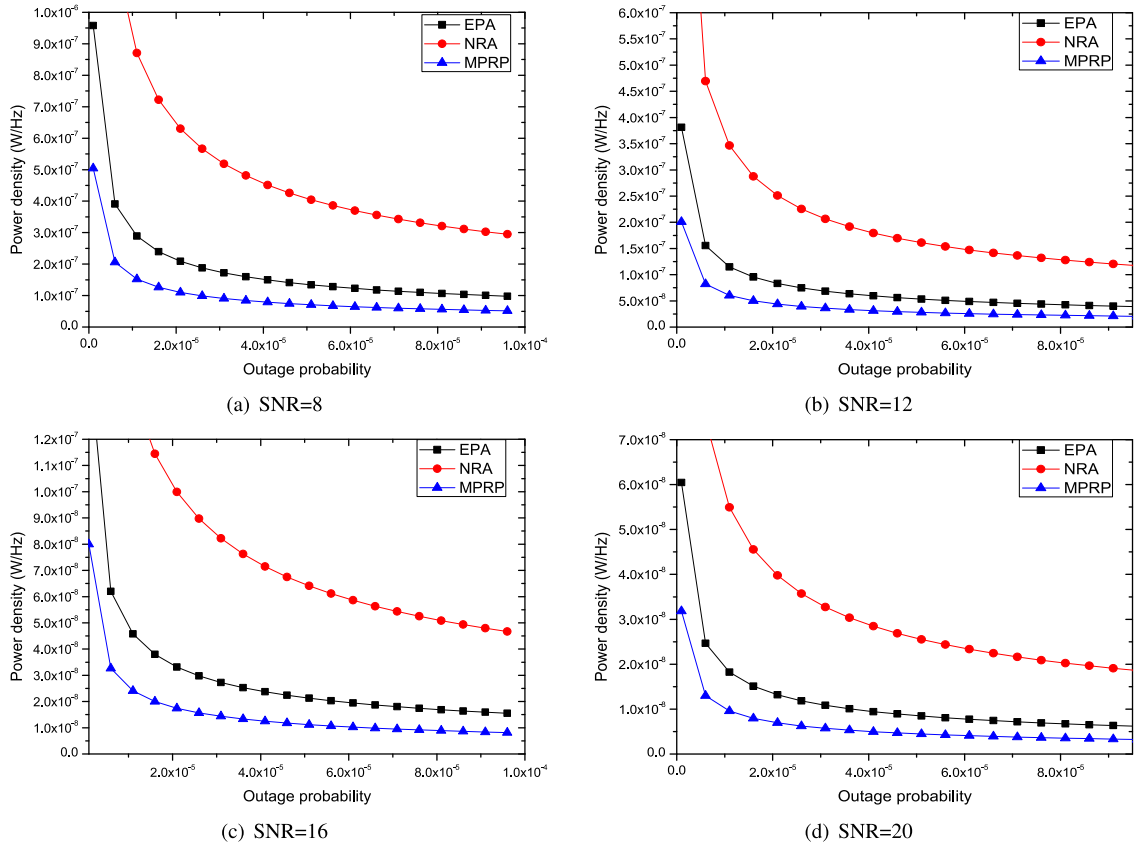

FIGURE 6. The effect of varying the P_{outMax} on the power density in EPA, NRA, MPRP. (a)-(d) represent the case under different SNR conditions, respectively. With the increase of the maximum allowable outage probability, the power density required by the three schemes gradually becomes smaller. The MPRP algorithm is not only smaller than the other two algorithms in the absolute value of the final required power density, but also tends to stabilize the inflection point earlier.

Thus $R_i\,(i = 0, 1 \ldots, n)$ can be taken into Eq. 39 in turn to calculate the minimum power density $\rho_i\,(i = 0, 1 \ldots, n)$. At the same time, the power allocation factors sequence $B_i\,(i = 0, 1 \ldots, n)$ satisfying the outage probability condition Eq. 35 under different number of relay nodes can be obtained. Then the total minimum power density can be obtained:

$$\rho_i = \min \rho = \frac{P_s + \sum_{j=1}^{i} P_j}{W},\ (i = 0, 1 \ldots, n),\quad s.t. P_{out} \le P_{outMax}, \tag{65}$$

$$\rho_{\min} = \min \rho_i. \tag{66}$$

Therefore, R_i and B_i corresponding to $\rho_{\min}$ is the optimal relay selection and power allocation factors sequence. After a round of algorithms to get the $\rho_{\min}$, if the system needs to add other new nodes into the algorithm, an incremental comparison method can be adopted. That is, we only need to get the new ρ_i and compare it with the $\rho_{\min}$ in the previous round of algorithms. Then the smaller value of the two is the new $\rho_{\min}$. Let the processing delay caused by power allocation be T. In this scenario, the processing delay caused by traditional exhaustive method (TEM) is $\left(\sum_{L=0}^{n} C_n^L + 1\right) T = (2^n + 1)\, T$, while the processing delay of our MPRP algorithm is only $(n + 2)\, T$. The steps of the MPRP algorithm are depicted in algorithm 1.

IV. NUMERICAL ANALYSIS

In this section, we evaluate the performance of the MPRP algorithm with respect to the channel model of WAIC system.

A. SIMULATION ENVIRONMENT

According to technical characteristics and spectrum requirements of WAIC systems in Table 1, we consider a network with 125 nodes over an space with a radius of 15 m in our experiment. The nodes are deployed following a uniform random distribution. System parameters in the NLOS scenario including channel parameters are shown in Table 3. The system parameters of our deployment environment are formulated according to Table 1 [11]. And the channel model parameters are formulated according to [22] and [32]. In order to simulate the characteristics of statistical channel model, we take the channel parameters of each link randomly within the specified range in [32]. Equal power allocation algorithm (EPA) [30] and no relay algorithm (NRA) are added as the control group, so as to better reflect the performance of MPRP algorithm. We have run each simulation experiment 100 times

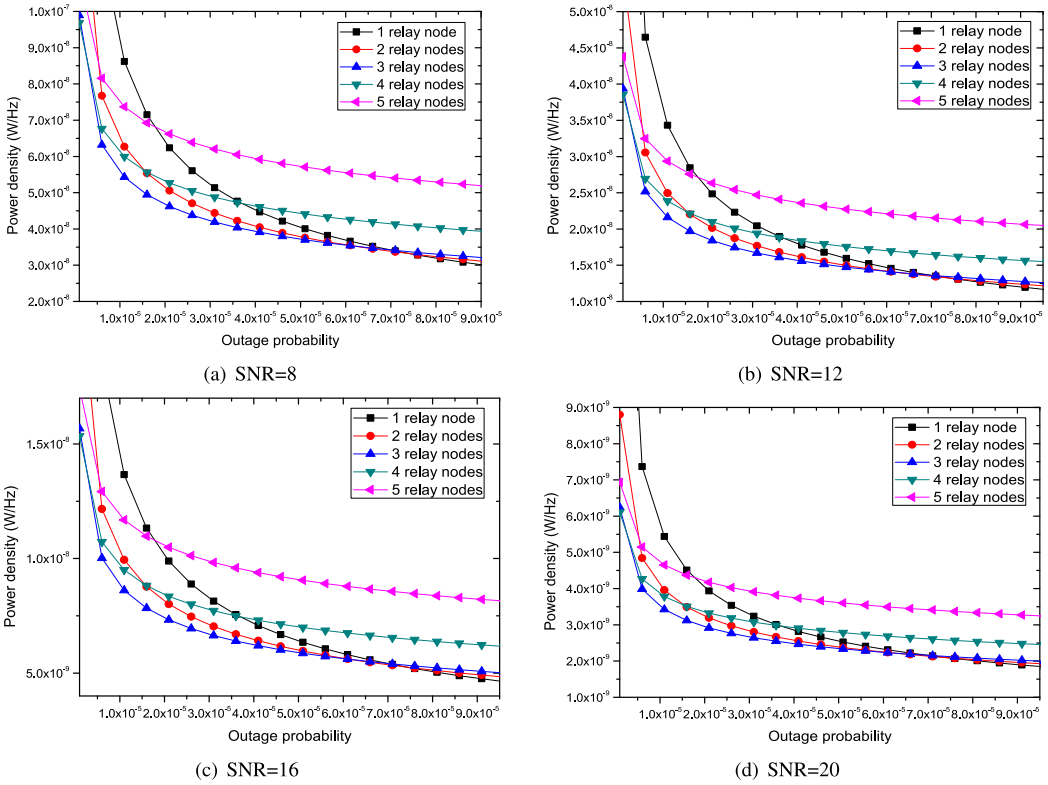

(a) SNR=8 (b) SNR=12

(c) SNR=16 (d) SNR=20

FIGURE 7. The effect of varying the relay nodes on the power density in MPRP. (a)-(d) represent the case under different SNR conditions, respectively. The power density decreases with increasing the maximum allowable outage probability.

Algorithm 1 MPRP

Input: $n, PL_0, \varepsilon_p, \sigma^2_{s,d}, \Lambda, \Gamma, Z_0, R, W, P_{outMax}, \sigma^2_{s,i}, \sigma^2_{i,d}, i = 1, \ldots, n$

Output: $P_{out}, \beta_0, \beta_i, \rho, B, R_i, B_i, \rho_i, \rho_{\min}, i = 1, \ldots, n$

1: Compute M_{sd}, M_{si}, M_{id} using Eq. 19, Eq. 26.
2: Get the expression of P_{out} using Eq. 17.
3: Expression of ρ is obtained by transforming P_{out}.
4: Get the Lagrange cost function $L(\beta_0, \beta_i)$ and nonlinear systems $F(x)$.
5: Compute B, R using Eq. 46, Eq. 47.
6: **if** ($\rho_{\min} = \emptyset$) **then**
7: Continue.
8: **else**
9: Obtain the ρ_i using Eq. 39 to Eq. 47
10: Update the $\rho_{\min}$ by getting the minimum values in the ρ_i and $\rho_{\min}$.
11: **end if**
12: Repeat Steps 1 to 4 obtain the B_i, R_i and ρ_i.
13: Update the minimum value $\rho_{\min}$ by compare each ρ_i.

and plotted the average result in the corresponding graph data point.

B. PERFORMANCE METRICS

The effectiveness of the proposed power allocation and relay selection approach are realized through examining the following 3 metrics: (*i*) System power density: Transmit power of source node and relay node divided by system frequency bandwidth. (*ii*) Outage probability: the probability that the link capacity cannot meet the required user rate. (*iii*) Algorithm processing delay: the time required for the optimal power allocation and relay selection algorithm.

TABLE 3. Simulation Parameters.

Parameter	Value
WAIC System classification	high data rate inside (HI)
Installation domain	inside
Wireless communication environment	NLOS
Space radius (n)	15 m
Number of nodes	125
Noise power density	-174 dBm/Hz
Number of relay hops	2
Center frequency (f)	4300 MHz
Frequency bandwidth (W)	200 MHz
Time slots per second	1.6×10^6
Average data rate (R)	1 bits/time slot
Maximum allowable outage probability (P_{outMax})	10^{-4}
Pathloss at the 1 m (PL_0)	36.6 - 51.4 dB
Pathloss exponent (ε_p)	1.63 - 3.07
Standard deviation (σ_S)	1.9 - 3.9
Cluster arrival rate (Λ)	41.2 - 208.3 ns
Cluster attenuation coefficient (Γ)	31.7 - 104.7 ns

C. SIMULATION RESULTS

1) EFFECT OF INCREASING SNR

In this section, we analyze the power density and outage probability of MPRP, EPA,NRA algorithm for various SNR in

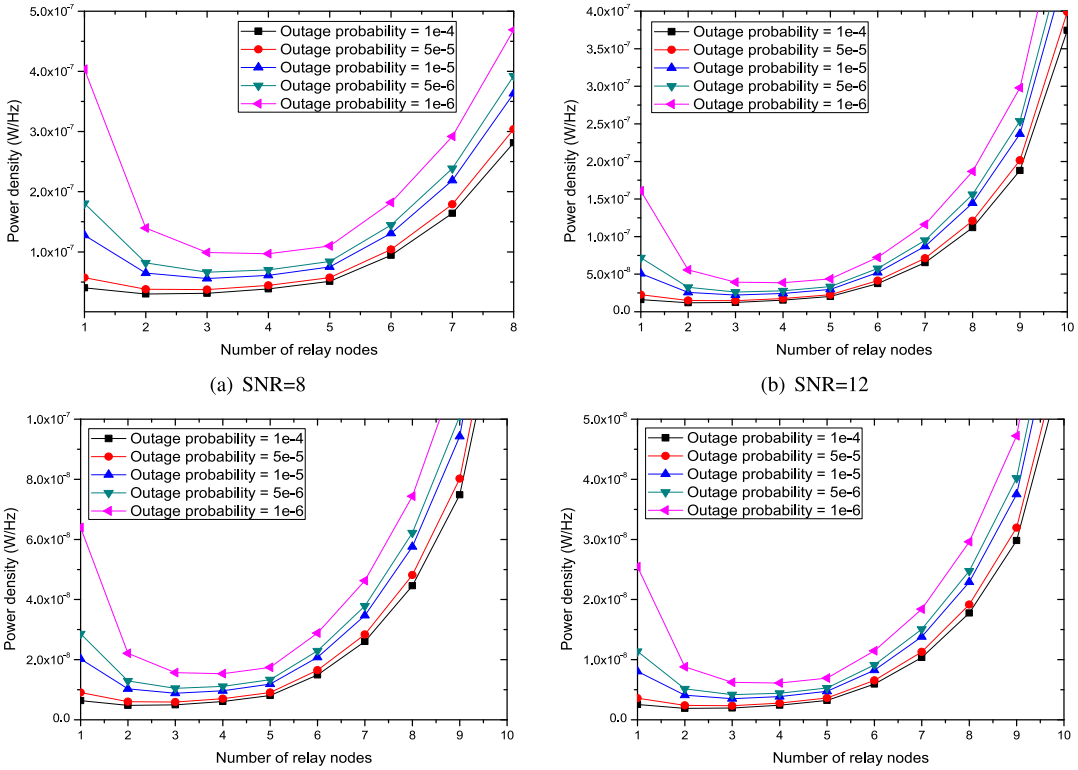

FIGURE 8. Power density of MPRP changing with the L under different P_{outMax}. (a)-(d) represent the case under different SNR conditions, respectively. With the increase of the number of relay nodes, the required power density first decreases, reaches the lowest point and then increases continuously.

the network. Firstly, the maximum allowable outage probability P_{outMax} is fixed at 10^{-4}, and the curves of power density ρ versus SNR in the 3 algorithms are observed.

From Fig. 5 we can notice that with higher SNR in the network, a good channel environment makes signal transmission easier and ultimately reduces the power density ρ required for all research methods to achieve P_{outMax}. However, EPA and MPRP algorithms require less power density than NRA algorithms. Since the NRA algorithm has no relay mechanism, the diversity gain can not be obtained. Also, NRA algorithm causes significant power density overhead under the condition of low SNR of the system. On the other hand, as the EPA algorithm allocates all relay nodes equal power, so that different channel conditions can not be properly processed separately, the flexibility of power allocation is lacking, and finally the power density required by the network is increased. However, MPRP algorithm distributes power according to the CSI of different links, which allocate higher power factors to links with better channel conditions and obtain a higher diversity gain. Hence, the power density required by the MPRP algorithm is lower.

As shown in Fig. 6, with the increase of the maximum allowable outage probability, which mean that the network requires lower transmission quality, the power density required by the three schemes gradually becomes smaller. Under P_{outMax} certain conditions, the required power density is eased to a certain extent. It is worth mentioning that under the condition of different SNR, the inflection point of the MPRP occurs when P_{outMax} is 1.2×10^{-5}. However, the inflection point of the EPA and NRA occur when P_{outMax} are 3.0×10^{-5} and 7.0×10^{-5} respectively. It means that the MPRP algorithm is not only smaller than the other two algorithms in the absolute value of the final required power density, but also tends to stabilize the inflection point earlier. Even for more stringent transmission quality requirements, MPRP can also reduce its required power density.

2) EFFECT OF INCREASING NUMBER OF RELAYS

In this section, we investigate the scalability of the studied MPRP algorithm by considering different number of relay nodes. We have plotted the system power density in Fig. 7, as a function of increasing P_{outMax} at different number of relay nodes. Similarly to Fig. 6, the power density decreases with increasing the maximum allowable outage probability, i.e., the reduced transmission requirement makes the required power density smaller. However, the curve will show some differences when the number of relay nodes is different in Fig. 7. We can see that two and three relay nodes is obviously superior to others when the P_{outMax} is less

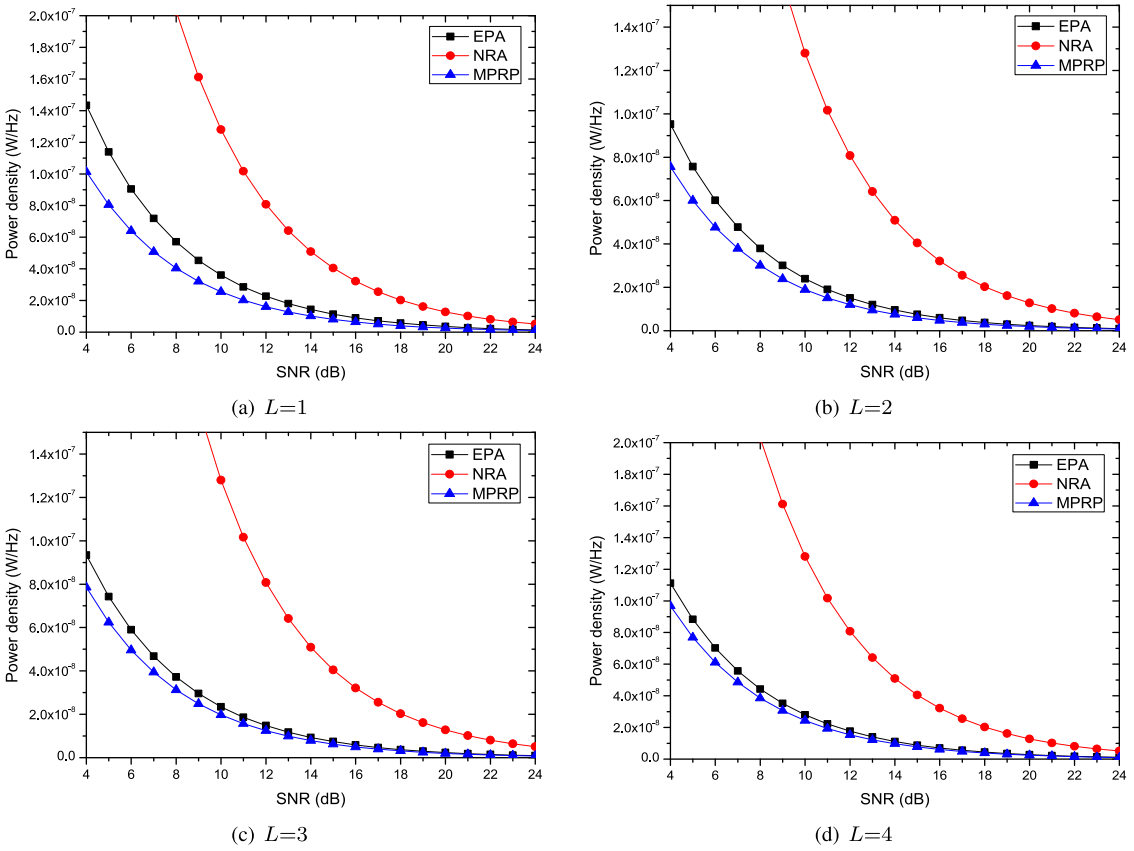

FIGURE 9. The effect of varying the SNR on the power density at different *L*. (a)-(d) represent the case under different *L* conditions, respectively. As the SNR increases, the power density required by EPA, NRA, MPRP decreases. As the number of relay nodes in the network changes, MPRP can use more efficient power allocation for forwarding amplification than EPA and NRA algorithm, thereby reducing power density.

than 6×10^{-5}. In addition, when only one relay node is used, the power density is small when the P_{outMax} probability is greater than 6.5×10^{-5}. When more than 4 relay nodes are involved, the transmission power loss is too large and the overall power density increases due to the excessive number of relay nodes.

To further confirm the influence of different number of relay nodes L, the L is taken as the abscissa and the ordinate is the system power density. In several different P_{outMax} cases, the most suitable number of relay nodes is obtained in various environments. As shown in Fig. 8, with the increase of the number of relay nodes, the required power density first decreases, reaches the lowest point and then increases continuously. It should be noted that no matter how SNR and P_{outMax} are set, the optimal number of relay nodes ranges from 2 to 4. Although the experimental result of power density are related to the channel parameters, the determination of the optimal number of nodes will not be affected. As a matter of fact, we can see that up to 4 nodes will participate in the relay. Thus, when calculating the optimal relay node set, the number of relay nodes L can be set to 4 at most, which further shortens the calculation time of the algorithm.

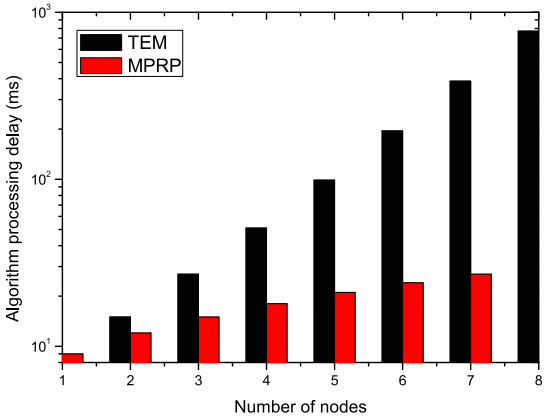

FIGURE 10. Processing delay of MPRP and TEM algorithm. The horizontal coordinate is the number of nodes and the vertical coordinate is Algorithm processing delay. The curve of TEM shows exponential growth, and the curve of the MPRP increases linearly. Compared with the typical TEM algorithm, the processing delay of the MPRP algorithm becomes more prominent as the number of nodes in the network increases.

Set the number of relay nodes from 1 to 4. As the number of relay nodes in the network changes, MPRP can use more efficient power allocation for forwarding amplification than

EPA and NRA algorithm, thereby reducing power density, as shown in Fig. 9. The data values plotted in Fig. 9 reveal that the proposed MPRP algorithm outperforms in terms of power density even in the case of multiple relay nodes.

3) PROCESSING DELAY OF MPRP

In Fig. 10, we have plotted the processing delay of MPRP and TEM algorithm by simulating the operation of the network. As can be seen from the Fig. 10, compared with the typical TEM algorithm, the processing delay of the MPRP algorithm becomes more prominent as the number of nodes in the network increases. After determining the power allocation factor sequence of n nodes, the MPRP algorithm only needs to calculate how many nodes are required to participate in the relay. Therefore, the computation time and processing delay of the network is reduced.

V. CONCLUSION

In this article, we apply the relay selection and power allocation method based on the minimum power density criterion to wireless avionics intra-communications (WAIC) systems with multiple relay nodes. The system power density can be efficiently reduced by the algorithm. The expression of outage probability in WAIC environment is derived, and the formula of minimum power density under the condition of maximum allowable outage probability is obtained. Furthermore, a new optimal relay node sequence selection and power allocation approach of source node and relay nodes has been developed based on Lagrange multiplier method and Quasi-Newton method. Finally, the MPRP algorithm was compared to two of the most common relay algorithms namely the EPA and TEM. A better performance of the proposed relay selection and power allocation algorithm has been shown through numerical examples. As part of the future work, the proposed algorithm can be extended to investigate the performance of multi-user and multi relay WAIC systems.

ACKNOWLEDGMENT

The authors would like to thank colleagues and experts for assistance in providing insights and suggestions. They would also like to thank the anonymous reviewers for carefully reading the article and providing constructive comments.

REFERENCES

[1] *Working Document Towards a Preliminary Draft New Report ITU- R M: Characteristics of Waic Systems and Bandwidth Requirements to Support Their Safe Operation*, document ITU-R WP5B Contribution, ITU Radiocommunication Study Groups, Geneva, Switzerland, Dec. 2013.

[2] H. Saghir, C. Nerguizian, J. J. Laurin, and F. Moupfouma, "In-cabin wideband channel characterization for WAIC systems," *IEEE Trans. Aerosp. Electron. Syst.*, vol. 50, no. 1, pp. 516–529, Jan. 2014.

[3] S. Futatsumori, N. Miyazaki, T. Hikage, T. Sekiguchi, M. Yamamoto, and T. Nojima, "Interference path loss measurements of beechcraft B300 aircraft at 4 GHz wireless avionics intra-communication band," in *Proc. Int. Symp. Electromagn. Compat. - EMC Eur.*, Sep. 2020, pp. 1–4.

[4] S. Futatsumori, K. Morioka, T. Hikage, T. Sekiguchi, M. Yamamoto, and T. Nojima, "Point source transmitting power estimation of wireless avionics intra-communication systems using the large-scale fdtd method," in *Proc. Int. Appl. Comput. Electromagn. Soc. Symp. (ACES)*, pp. 1–2, 2019.

[5] A. Baltaci, S. Zoppi, W. Kellerer, and D. Schupke, "Evaluation of cellular technologies for high data rate WAIC applications," in *Proc. IEEE Int. Conf. Commun. (ICC)*, May 2019, pp. 1–6.

[6] A. Baltaci, S. Zoppi, W. Kellerer, and D. Schupke, "Evaluation of cellular IoT for energy-constrained WAIC applications," in *Proc. IEEE 2nd 5G World Forum (5GWF)*, Sep. 2019, pp. 359–364.

[7] F. Liu, A. Garcia-Rodriguez, C. Masouros, and G. Geraci, "Interfering channel estimation in radar-cellular coexistence: How much information do we need?" *IEEE Trans. Wireless Commun.*, vol. 18, no. 9, pp. 4238–4253, Sep. 2019.

[8] *ITU-R Technical Characteristics and Operational Objectives for Wireless Avionics Intra- Communications (WAIC)*, document ITU-R REPORT M.2197, Radiocommunication Study Groups, Nov. 2010.

[9] D. C. Malocha and S. Malocha, "SAW sensor development at 4.3 GHz for the wireless avionics intra-communications band," in *Proc. IEEE Int. Ultrason. Symp. (IUS)*, Oct. 2019, pp. 619–622.

[10] P. Park and W. Chang, "Performance comparison of industrial wireless networks for wireless avionics intra-communications," *IEEE Commun. Lett.*, vol. 21, no. 1, pp. 116–119, Jan. 2017.

[11] *Technical Characteristics and Spectrum Requirements of Wireless Avionics Intra-Communications Systems to Support Their Safe Operation*, document ITU-R M.2283-0, 2013.

[12] *Consideration of the Aeronautical Mobile (Route), Aeronautical Mobile, and Aeronautical Radio Navigation Services Allocations to Accommodate Wireless Avionics Intra-Communication (waic)*, document Report M.2318, ITU, Nov. 2014.

[13] A. Dwivedi, S. Zoppi, W. Kellerer, F. Neubauer, and D. Schupke, "Wireless avionics intra-communication (WAIC) QoS measurements of an ultra wideband (UWB) device for low-data rate transmissions," in *Proc. AIAA/IEEE 39th Digit. Avionics Syst. Conf. (DASC)*, Oct. 2020, pp. 1–10.

[14] W.-P. Nwadiugwu and D.-S. Kim, "Ultrawideband network channel models for next-generation wireless avionic system," *IEEE Trans. Aerosp. Electron. Syst.*, vol. 56, no. 1, pp. 113–129, Feb. 2020.

[15] D.-K. Dang, A. Mifdaoui, and T. Gayraud, "Fly-By-Wireless for next generation aircraft: Challenges and potential solutions," in *Proc. IFIP Wireless Days*, Nov. 2012, pp. 1–8.

[16] P. Park, P. Di Marco, J. Nah, and C. Fischione, "Wireless avionics intra-communications: A survey of benefits, challenges, and solutions," *IEEE Internet Things J.*, early access, Nov. 18, 2020, doi: 10.1109/JIOT.2020.3038848.

[17] N. Raharya and M. Suryanegara, "Compatibility analysis of wireless avionics intra communications (WAIC) to radio altimeter at 4200–4400 MHz," in *Proc. IEEE Asia Pacific Conf. Wireless Mobile*, Aug. 2014, pp. 17–22.

[18] A. Ameti, R. J. Fontana, E. J. Knight, and E. Richley, "Ultra wideband technology for aircraft wireless intercommunications systems (AWICS) design," *IEEE Aerosp. Electron. Syst. Mag.*, vol. 19, no. 7, pp. 14–18, Jul. 2004.

[19] R. Samano-Robles, E. Tovar, J. Cintra, and A. Rocha, "Wireless avionics intra-communications: Current trends and design issues," in *Proc. 11th Int. Conf. Digit. Inf. Manage. (ICDIM)*, Sep. 2016, pp. 266–273.

[20] *Operational and Technical Characteristics and Protection Criteria of Radio Altimeters Utilizing the Band 4200-4400 MHz*, document ITU-R M.2059-0, 2014.

[21] M. Suryanegara and N. Raharya, "Modulation performance in wireless avionics intra communications (WAIC)," in *Proc. 1st Int. Conf. Inf. Technol., Comput., Electr. Eng.*, Nov. 2014, pp. 434–437.

[22] D.-K. Dang, A. Mifdaoui, and T. Gayraud, "Design and analysis of UWB-based network for reliable and timely communications in safety-critical avionics," in *Proc. 10th IEEE Workshop Factory Commun. Syst. (WFCS)*, May 2014, pp. 1–10.

[23] E. International, R. Rhône, and C.-G. T/f, "High rate ultra wideband phy and mac standard," Ecma Int., Geneva, Switzerland, Tech. Rep. ECMA-368, 2007.

[24] G. N. Shirazi, P.-Y. Kong, and T. C. Khong, "Optimal cooperative relaying schemes in IR-UWB networks," *IEEE Trans. Mobile Comput.*, vol. 9, no. 7, pp. 969–981, Jul. 2010.

[25] J. N. Laneman, D. N. C. Tse, and G. W. Wornell, "Cooperative diversity in wireless networks: Efficient protocols and outage behavior," *IEEE Trans. Inf. Theory*, vol. 50, no. 12, pp. 3062–3080, Dec. 2004.

[26] J. N. Laneman and G. W. Wornell, "Distributed space-time coded protocols for exploiting cooperative diversity in wireless networks," in *Proc. Global Telecommun. Conf., GLOBECOM*, Nov. 2002, pp. 77–81.

[27] A. Sendonaris, E. Erkip, and B. Aazhang, "User cooperation diversity—Part I: System description," *IEEE Trans. Commun.*, vol. 51, no. 11, pp. 1927–1938, Nov. 2003.
[28] J. Ding, E. Dutkiewicz, X. Huang, and G. Fang, "Energy-efficient cooperative relay selection for UWB based body area networks," in *Proc. IEEE Int. Conf. Ultra-Wideband (ICUWB)*, Sep. 2013, pp. 97–102.
[29] J. Chen, L. Clavier, Y. Xi, A. Burr, N. Rolland, and P. Rolland, "α-stable interference modelling and relay selection for regenerative cooperative IR-UWB systems," in *Proc. 3rd Eur. Wireless Technol. Conf.*, Sep. 2010, pp. 81–84.
[30] Z. Ding, S. M. Perlaza, I. Esnaola, and H. V. Poor, "Power allocation strategies in energy harvesting wireless cooperative networks," *IEEE Trans. Wireless Commun.*, vol. 13, no. 2, pp. 846–860, Feb. 2014.
[31] A. Khan and D.-S. Kim, "Cooperative relay selection scheme for IR-UWB networks in avionic system," in *Proc. KICS Summer*, Jun. 2016, pp. 190–191.
[32] J. Foerster, *Channel Modeling Sub-Committee Report Final*, document p802.15-02/368r5-SG3a, Jan. 2003.
[33] L.-Y. Sun, X.-H. Zhao, and M. Guo, "Outage probability based power allocation and relay selection algorithm in cooperative communication," *Tongxin Xuebao/J. Commun.*, vol. 34, pp. 84–91, Oct. 2013.
[34] Y. Zhao, R. Adve, and T. Joon Lim, "Improving amplify-and-forward relay networks: Optimal power allocation versus selection," *IEEE Trans. Wireless Commun.*, vol. 6, no. 8, pp. 3114–3123, Aug. 2007.
[35] R. Albu, A. Lecointre, D. Dragomirescu, T. Gayraud, and P. Berthou, "Evaluation of uwb communication for in-flight entertainment system in the aircraft cabin," *IFAC Proc. Volumes*, vol. 40, no. 22, pp. 49–56, 2007.
[36] L. Richard, *Numerical Analysis*, 9th ed. , Boston, MA, USA: Cengage Learning, Brooks/Cole, 1997.

YUANJUN ZUO (Graduate Student Member, IEEE) was born in 1993. He received the B.S. and M.S. degrees from the Beijing Institute of Technology, China, in 2014 and 2017, respectively. He is currently pursuing the Ph.D. degree in communication and information system with the School of Electronic Information Engineering, Beihang University, China.

His current research interests include wireless communication, wireless sensor networks, wireless avionics intra-communication, and avionics systems. He is a member of the IEEE Communications Society, the IEEE Signal Processing Society, and the IEEE Aerospace and Electronic Systems Society.

QIAO LI (Member, IEEE) received the Ph.D. degree in communication systems from Beihang University, Beijing, China, in 2005. He is an Assistant Professor with the School of Electronics and Information Engineering, Beihang University.

He had been in charge of one general project of NSFC and two aviation science foundation projects. In terms of international exchanges and cooperation, in 2013, as a major member, he took part in the establishing of the Beihang-TTTech Time-Triggered Technology Joint Laboratory. His research interests include digital communication technologies, avionics systems, and real-time networks.

GUANGSHAN LU received the Ph.D. degree from Beihang University, Beijing, China.

He has been a Professor with the School of Electronics and Information Engineering, Beihang University. He received nearly 30 national science and technology progress awards, national defense science and technology progress awards and group company science and technology progress awards, published more than 40 articles, and received the first-class merit of group company for many times. His research interests include avionics systems integration and fire control systems. He had successively presided over the research and development many types of photoelectric systems.

HUAGANG XIONG received the Ph.D. degree in communication and information system from the School of Electronic Information Engineering, Beihang University, China, in 1998.

He is currently a Full Professor with Beihang University, where he is also the Chief of BUAA-TTTech Time-Triggered Technology Joint Laboratory (TTTJL). He is also the Head of the Avionics and Bus Communications Research Team (ABC), School of Electronic Information Engineering, Beihang University. He has published more than 305 peer-reviewed articles which are indexed by SCI or EI and 3 books. He has presided more than 20 major projects in total, such as the National Natural Science Foundation of China, National 863 Program, and Civil Aircraft Research. His research interests include communication network theory and technology, avionics information integration, airborne networks, and standards.

Prof. Xiong is a member of the China Aviation Electronics Standardization Committee, also the Director of the Beijing Electronic Circuit Research Association, a member of the Avionics and Air Traffic Control Branch of China Society of Aeronautics and Astronautics, and an Expert of the Civil Aircraft Scientific Research Group.